Journal of Membrane Science 612 (2020) 118406

Contents lists available at ScienceDirect

Journal of Membrane Science

journal homepage: http://www.elsevier.com/locate/memsci

Hydrogen-sieving single-layer graphene membranes obtained by crystallographic and morphological optimization of catalytic copper foil

Mojtaba Rezaei, Shaoxian Li, Shiqi Huang, Kumar Varoon Agrawal *

Laboratory of Advanced Separations, École Polytechnique Fédérale de Lausanne, Sion, Switzerland

ARTICLE INFO

Keywords:
Gas sieving
Single-layer graphene
Cu foil
Chemical vapor deposition
Intrinsic defects

ABSTRACT

Gas separation membranes based on single-layer-graphene are highly attractive because the size of graphene nanopores can be tuned to separate gases by the size-sieving mechanism. A prerequisite for this, the synthesis of high-quality polycrystalline single-layer graphene film by chemical vapor deposition (CVD), is extremely crucial. The quality of graphene in the context of membranes is reflected by the size and the density of the intrinsic vacancy defects, and is affected by the catalytic metal substrate and the CVD environment. Generally, expensive high-purity Cu foil is used to obtain gas-sieving performance from single-layer graphene. For the eventual scale-up of graphene membranes, it is highly attractive to use low-cost Cu foils, however, as we show here, these Cu foils are rough and graphene membranes derived from these foils do not yield gas-sieving performance. Herein, we conduct a systematic high-temperature annealing study on two separate, commercial, low-cost Cu foils leading to their transformation to Cu(111). The annealing process smoothened the Cu surface, decreasing the root mean square (RMS) surface roughness from over 200 nm to close to 100 nm. The RMS roughness on the individual Cu step, measured using the scanning tunneling microscopy (STM), was only 0.23 nm. The smooth, oriented Cu grains yielded single-layer graphene with a significantly lower defect density with I_D/I_G ratio decreasing from 0.18 ± 0.02 to 0.04 ± 0.01. Finally, single-layer graphene films, synthesized on the annealed low-purity Cu foil, yielded H_2-selective membranes with H_2 permeance reaching 1000 gas permeation units (GPU) in combination with attractive H_2/CH_4 and H_2/C_3H_8 selectivities of 13 and 26, respectively.

1. Introduction

Single-layer graphene hosting subnanometer-sized nanopores have shown attractive gas separation performances by molecular sieving where separation takes places based on differences in size of the molecule [1–5]. The ultrashort diffusion path of gas molecules across the sieving nanopore, involves only one rate-limiting transition state when the molecule arrives at the center of the nanopore [6]. With a narrow pore-size-distribution (PSD) in graphene, this manifests in a selective gas flux [7,8]. The development of graphene-based membranes is gaining momentum from the fact that the size of graphene nanopores can be tuned, increased or decreased, in a controlled fashion by various chemical or physical etching techniques and post-synthetic functionalization [9]. For example, recently, we reported an angstrom resolution in differentiating gas molecules [10]. Further advances in pore-size engineering, for example, by developing a self-limiting etching condition, is likely to allow sub-angstrom resolution in molecular differentiation.

For membrane-based separation, graphene is almost always synthesized by the chemical vapor deposition (CVD) method [11,12], mainly because the CVD synthesis can be carried out rapidly on the m^2-scale, and is conducive to scale-up. Synthesis of graphene in a roll-to-roll basis by CVD has been already demonstrated [13,14]. For the synthesis of single-layer graphene, Cu foil is the preferred catalytic substrate because Cu has a low carbon solubility (<0.001 atomic%) and graphene synthesis proceeds predominantly by nucleation and growth on the Cu surface, which is referred to as the surface-diffusion-directed growth mechanism [15]. Typical grain growth rates of 1-10 μm/min have been reported [16]. Once a polycrystalline film is formed, the growth is somewhat self-limiting with respect to the exposure time of the carbon precursor. In contrast, on metals with high carbon solubility (e.g., Ni), a carbon reservoir is formed at high temperature and a multilayer graphene film is precipitated during the cooling step [12].

Typically, a small population of intrinsic vacancy-defects is incorporated in the graphene lattice during CVD. These defects have origin in an incomplete intergrowth of misaligned grains [17,18] as well as the

* Corresponding author.
E-mail address: kumar.agrawal@epfl.ch (K.V. Agrawal).

https://doi.org/10.1016/j.memsci.2020.118406
Received 9 April 2020; Received in revised form 14 June 2020; Accepted 15 June 2020
Available online 4 July 2020

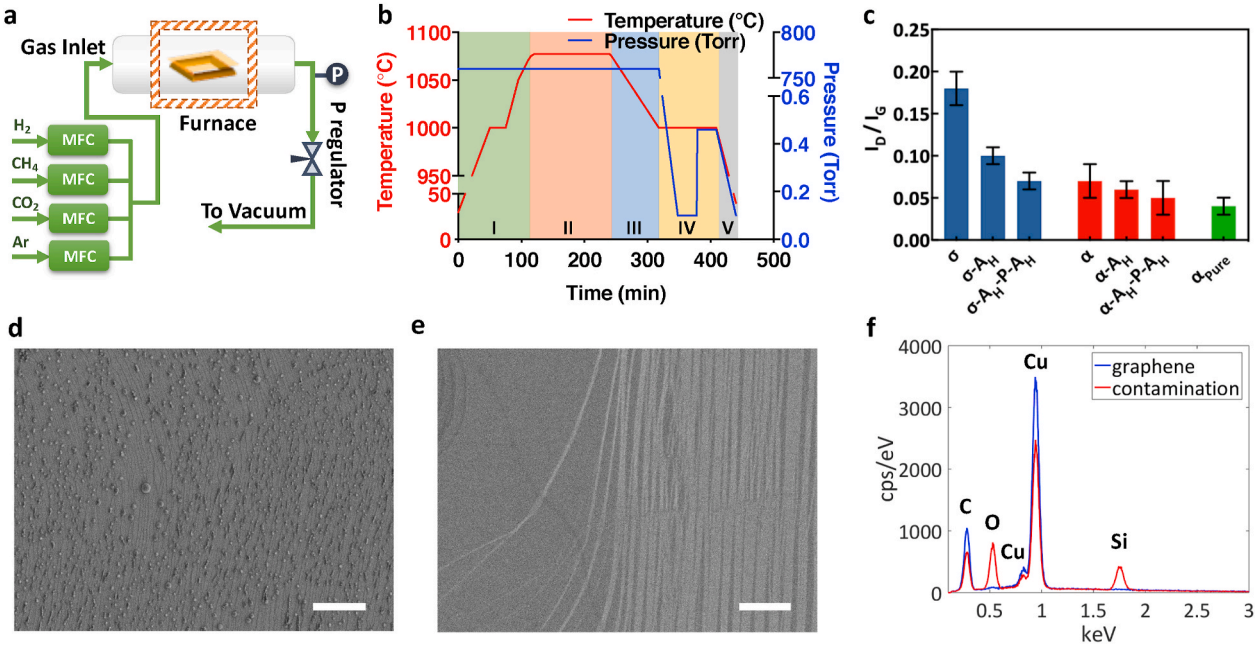

Fig. 1. a) Schematic of the setup for annealing Cu and LPCVD of graphene. b) Temperature and pressure profiles as a function of time for the high-temperature annealing of Cu, and subsequent synthesis of graphene. The colored sections refer to the following: I) removal of organic contaminations by CO_2 at 1000 °C, II) heating foil at 1077 °C, III) controlled cooling at 1 °C/min, IV) LPCVD of graphene, and V) rapid cooling to stop crystallization. c) I_D/I_G ratio in the Raman spectra of graphene synthesized on as-received as well as thermally-annealed and polished Cu foils. The error bar represents the standard deviation in the I_D/I_G ratio obtained by mapping (16 spectra or more). SEM images of the graphene grown on commercial Cu inside a quartz reactor (d), and inside the quartz reactor lined with the alumina tube (e). The scalebar is 2 μm. f) EDX analysis of the particles in (d).

etching of graphene lattice in the presence of oxygen leak in the CVD reactor [19]. Nevertheless, the vacancy-defects that have missing 10–16 carbon atoms can be attractive for gas separation by the size-sieving mechanism [7,8]. For example, Huang et al. reported that as-synthesized graphene with a low-density (0.025%) of intrinsic defects can separate H_2 from CH_4 with selectivity up to 25 [20]. Kidambi et al. showed that by reducing the CVD temperature to 900 °C, the density of intrinsic subnanometer-sized vacancy-defects could be increased [21]. Yuan et al. investigated gas transport from intrinsic defects in as-synthesized graphene on electropolished Cu foil and reported the evidence of molecular sieving [22]. Khan et al. reported that H_2-sieving vacancy defects can be incorporated in graphene at lower CVD temperature when benzene is chosen as the carbon precursor [23]. Most of these studies used expensive high-purity Cu foil with prohibitive cost for scaling-up graphene membranes. In fact, as we show here, as-received low-cost, low-purity polycrystalline Cu foils do not lead to high-quality graphene membranes attributing to high surface roughness and mixed crystallographic orientation of the as-received foils. Therefore, optimization of the low-cost Cu foils is crucial to realize a scalable production of the gas-sieving graphene membranes.

Herein, we demonstrate a facile crystallographic and morphological optimization protocol, applied to two different low-cost Cu foils, which successfully transforms them into smooth Cu(111) substrates, resulting in the synthesis of higher-quality single-layer graphene which ultimately led to hydrogen-sieving membranes. Briefly, a slow and controlled annealing close to the melting point of the Cu was carried out which annealed the Cu grains orienting them along the (111) out-of-plane direction. The high-temperature annealing also smoothened the Cu surface, with root-mean-square (RMS) roughness over a large area down to ca. 100 nm, and on a single Cu step as low as 0.23 nm. This treatment greatly improved the gas separation performance from the intrinsic defects of graphene membranes. For example, before the optimization of Cu foil, gas selectivities were close to those expected from the Knudsen transport, indicating the domination of large non-sieving vacancy-defects in graphene. After the treatment of the Cu foil, attractive H_2/CH_4 and H_2/C_3H_8 selectivities of 13 and 26, respectively, were achieved along with a H_2 permeance of 1000 GPU (1 GPU = 3.35×10^{-10} mol m^{-2} s^{-1} Pa^{-1}). We attribute this to (i) smoothened surface of Cu foil post-annealing, and (ii) crystallographic re-orientation to Cu(111). This is because the smoothened Cu surface facilitates fabrication of high-quality membranes by perhaps avoiding nanoscale cracks during the graphene transfer step. The Cu(111) surface reduces the grain-boundary defects attributing to the fact that there is only a small mismatch (3–4%) between the lattice constants of the (111) facet of Cu and that of graphene [24,25].

2. Experimental

2.1. Annealing and smoothening of commercial Cu foils

Heat treatment of the commercial Cu foils was carried out in a three-zone high-temperature furnace equipped with a high-purity alumina tube (99.8% purity, diameter: 5 cm, length: 1.2 m, MTI Corp.) housed inside a fused quartz tube (diameter: 6 cm, length: 1.4 m, MTI Corp.) as shown in Fig. S1. The quartz tube was used for making leak-tight connections with the gas lines and the vacuum source, whereas the alumina tube was used to prevent the silica contamination, originating from quartz tube, onto graphene. In each run, a piece of Cu foil (2×5 cm^2) was placed on a high-purity alumina boat (99.8% purity, Almath Crucibles Ltd) and was heated to 1000 °C. The organic contaminants on the foil were removed by treating the sample at 1000 °C and 800 torr in a CO_2 atmosphere for 30 min. Then, the system was evacuated and was filled with H_2/Ar (1:10) to the pressure of 1 bar. After this, annealing was performed by two methods. In the first method, referred to as high-temperature annealing or A_H, the foil was heated at 1077 °C for 1 h. After this, the temperature was reduced at a rate of 1 °C/min to 1000 °C. In the second method, referred to as low-temperature annealing or A_L, the foil was just annealed at 1000 °C for 1 h. Post annealing, the foil was either cooled down to room temperature for further characterization or was immediately used to synthesize graphene. Optionally, the foils were

also polished to further smoothen their surface. Polishing was carried out using a mechanical polisher (UNIPOL-1210, MTI Corp.) for 10 min using a diamond polishing paste (particle size of ca. 0.25 μm, MTI Corp.). After polishing, foils were rinsed by deionized (DI) water and, subsequently, were cleaned by sonication treatment in isopropyl alcohol (4 times for 10 min).

2.2. Graphene synthesis

Single-layer graphene was synthesized by the low-pressure chemical vapor deposition (LPCVD) [20] on three separate kinds of 25-μm-thick Cu foils (Fig. 1a). Two kinds of foil from Alfa Aesar, with purities of 99.8% and 99.999% were used. These are referred to as α and α_{pure}, respectively. Another foil with a purity of 99.98% was sourced from Sigma Aldrich and is referred to as σ. Briefly, for LPCVD, a piece of as-received or annealed Cu foil (2×5 cm^2) was placed inside the reactor and was treated at 1000 °C and 800 Torr in CO_2 atmosphere for 30 min to remove the organic contaminations. Then, the reactor was evacuated to 1 mTorr, and subsequently, 8 sccm of H_2 was introduced for 30 min, increasing the pressure to 80 mTorr, to anneal the Cu surface and to reduce the surface oxides. Finally, 24 sccm of CH_4 was added for 30 min to synthesize a polycrystalline graphene film. In the end, the CH_4 flow was cut off while maintaining the H_2 flow, and the foil was pulled out of the heating zone to stop the crystallization.

2.3. Homemade Cu foil

Smooth Cu foils were synthesized by the template-stripping strategy [26] using a combination of thermal- and electro-deposition techniques. First, a 1-μm-thick Cu film was deposited on a Si wafer (300 nm SiO_2 top layer) by thermal evaporation (Edwards Auto 306 thermal evaporator) of 99.999% purity Cu pellets (Kurt J. Lesker) at 10^{-6} mbar. The deposition rate was ca. 1 nm/s. Next, following the report of Procházka et al. [27], ca. 25-μm-thick Cu film was electrodeposited on top, increasing the mechanical robustness of the film for handling and further processing. Briefly, the electrodeposition was carried out in an acidic $CuSO_4$ solution prepared by mixing $CuSO_4$ powder (purity>99%), H_2SO_4 solution, and deionized water to achieve a pH of ca. 2.3. A piece of Cu foil (2.5 cm × 5 cm, thickness: 0.127 mm, purity: 99.9%, Alfa Aesar) was used as the anode. The cathode (evaporated Cu) was placed 1.5 cm from the anode (Fig. S2). Electrodeposition was carried out at 60 °C by applying 0.3 V in a constant voltage mode leading to a current density of ca. 20 mA/cm^2 and a deposition rate of ca. 20 μm/h. After 75 min, the sample was removed from the solution and was rinsed by DI water before letting it dry at room temperature. Finally, the Cu foil was gently peeled off from the Si/SiO_2 substrate for further characterization and graphene synthesis.

2.4. Membrane fabrication

The graphene membranes were fabricated using a nanoporous carbon (NPC)-assisted method reported in the previous study (Fig. S3) [20]. Briefly, a solution of 0.1 g block copolymer, poly(styrene-b-4-vinyl pyridine) and 0.2 g turanose in dimethylformamide (DMF) was aged in an autoclave at 180 °C for 3 h to form a precursor solution. Then, the as-synthesized graphene on Cu was spin-coated (2 min at 2000 rpm) with the precursor solution. The film was pyrolyzed in Ar/H_2 atmosphere at 500 °C for 1 h, yielding the NPC film. Subsequently, the underlying Cu foil was etched using 0.2 M sodium persulfate solution, and the floating graphene/NPC film was rinsed with DI water several times before transferring it onto a porous tungsten support, fabricated by drilling 2500 5-μm-sized holes in a W foil using a high-energy laser (Potomac Photonics LLC).

Two graphene membranes were fabricated using a poly(1-trimethylsilyl-1-propyne) (PTMSP) assisted method reported in the previous study [28]. Briefly, a thin PTMSP film was coated onto the top of graphene on Cu by spin-coating as mechanical support, in order to prevent the graphene film from cracking during the transfer step. For this, a 1.25 wt% of PTMSP solution in toluene was spread on the graphene on Cu, followed by spinning at 1000 rpm for 30 s, and then 2000 rpm for 30 s. The resulting film was dried in ambient conditions for 12 h, and then in a vacuum oven for 12 h at room temperature. Subsequently, the underlying Cu foil was etched using 1 M $FeCl_3$ solution, and the floating graphene/PTMSP film was rinsed with DI water several times before transferring it onto a porous tungsten support.

2.5. Characterization

Scanning electron microscopy (SEM) images were acquired by FEI Teneo scanning electron microscope at an operating voltage of 1-2 kV and a working distance of 3-7 mm. Micro-Raman spectroscopy was carried out using Reinshow inVia™ instrument equipped with a 457 nm excitation source to directly characterize as-synthesized graphene on Cu. A 100× objective lens yielding a spot size of ca. 1 μm was used. The laser power was kept below 1 mW to reduce the localized heating led damages to graphene. Typically, 16 or more spectra were collected for each sample. After the background subtraction, the acquired data were analyzed using MATLAB.

X-ray diffraction (XRD) measurements were carried out in a Bruker D8 Discover X-ray diffractometer equipped with a laser-based alignment system. Surface roughness measurements were performed by Bruker DektaXT stylus profilometer with a 2-μm stylus radius and 3 mg force. The Bruker Vision64 v5.51 software was used for data processing.

The gas permeation tests were performed in a homemade permeation setup (Fig. S4) consisting of a leak-tight membrane module (details are reported in the previous studies [10,20]). Briefly, the W support was sandwiched between the Swagelok VCR fittings as a gasket. The setup was housed inside a temperature-controlled oven. Ar at 1 bar was used as the sweep gas. The permeation measurements were carried out for H_2, CH_4, C_3H_8, and SF_6 gases in a single-component mode with a feed pressure of 2 bar. A pre-calibrated mass spectrometer (Hiden Analytical, HPR-20) was used to analyze the permeate stream. Before measurements, membranes were heated to 150 °C to desorb the atmospheric contaminants.

STM was carried out by the Createc low-temperature scanning tunneling microscope at 77 K and 2×10^{-10} mbar. Before imaging, the Cu foil was annealed at 673 K for 30 min inside the STM chamber to clean the surface from contaminations. The image tilt was reduced by flattening in Gwyddion software.

3. Results and discussion

Single-layer graphene was synthesized on as-received Cu as well as Cu subjected to various annealing and polishing steps (Fig. 1a and b). The commercial Cu foil is usually rough hosting several micron-sized grooves attributing to the mechanical rolling process involved in the production of thin foils. Further, the surface of Cu is decorated with surface oxides [23,29]. As a result, thermal annealing of the foil is required to grow high-quality graphene [30]. Extended annealing near or above the melting point of Cu has shown to smoothen the Cu surface which in turn can improve the grain-alignment and reduces the nucleation density, and therefore, can reduce the grain-boundary

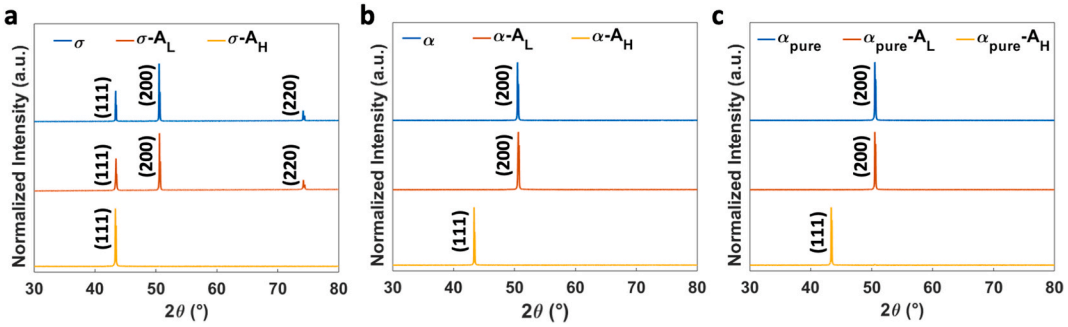

Fig. 2. XRD patterns of as-received Cu (blue trace), Cu annealed at 1000 °C during LPCVD (red trace), and Cu exposed to high-temperature annealing (orange trace). The results on σ, α, and α_{pure} samples are shown in (a), (b), and (c), respectively. (For interpretation of the references to color in this figure legend, the reader is referred to the Web version of this article.)

defects. Further, controlled annealing leads to a reorientation of Cu grains to (111) out-of-plane direction attributing to a lower surface energy of these facets [31,32]. In this work, we investigated the effect of high-temperature annealing on the intrinsic vacancy-defects in CVD graphene and subsequently the gas sieving performance. Two separate as-received low-cost Cu foils (α and σ) were studied and contrasted to high-cost, high-purity Cu foil (α_{pure} with 99.999% purity). When annealing or polishing was carried out, the corresponding sequence is indicated in the nomenclature of the foil. For instance, the high-temperature-annealed α foil is referred to as α-A_H. Similarly, the sequence of high-temperature-annealing/polishing/high-temperature-annealing on the α foil is referred to as α-A_H-P-A_H.

3.1. Intrinsic defects in graphene

Graphene was synthesized in the presence of H_2 to minimize the defects caused by the unavoidable leakage of atmospheric O_2 into the evacuated CVD reactor [19]. Raman spectroscopy was used to quantify the density of intrinsic defects and the overall quality of as-synthesized graphene. Consistent with the literature, three characteristic peaks were observed in the Raman spectra: D peak near 1350 cm^{-1}, G peak near 1585 cm^{-1}, and $2D$ peak near 2700 cm^{-1}. The estimation of defect density was carried out by using the carbon amorphization trajectory [33,34], by investigating the ratio of the intensities of D and G peaks, i.e. I_D/I_G. This is mainly because the D peak is activated in the presence of symmetry-breaking or symmetry-distorting defects such as sp^3-sites or carbon vacancies [34].

As-synthesized graphene films with different annealing/polishing history of the Cu foils were analyzed. When the annealing was not carried out, the α_{pure} foil yielded the lowest I_D/I_G ratio (0.04 ± 0.01), followed by α foil (0.07 ± 0.02). The σ foil yielded a much higher I_D/I_G ratio (0.18 ± 0.02). As we show later, this has roots in the grain-orientation and surface roughness of the Cu foils. When the foils were subjected to annealing/polishing steps, the defect density in graphene could be reduced (Fig. 1c). The trends were similar for all low-purity Cu foils. After the high-temperature annealing (1077 °C for 1 h followed by cooling to 1000 °C at 1 °C/min), the I_D/I_G ratio from the resulting graphene decreased significantly (Fig. 1c). Polishing the low-purity Cu surface followed by high-temperature annealing further reduced the defect density. Overall, the low-cost foils could be modified by annealing and polishing (α-A_H-P-A_H) to yield I_D/I_G ratio comparable to that from α_{pure}. To understand the reason behind the obtained results, crystallographic and morphological changes in the Cu foil were studied and are discussed in the next sections.

We would like to note that the Cu annealing was carried in a furnace lined with high-purity alumina tube (Fig. S1) to prevent build-up of SiO_x particles on the surface of Cu [35,36]. Briefly, the phase transition (α/β) of quartz at 573 °C allows Cu atoms and hydrocarbon to diffuse into the quartz tube, leading to the release and the precipitation of the SiO_x particles onto the Cu foil and graphene. The density of SiO_x particles on the surface increases by repeated usage of the quartz tube. By adding the high-purity alumina tube inside the quartz tube, the number of particles could be significantly reduced (Fig. 1d, e, f).

3.2. The orientation of Cu grains

The in-plane orientation and intergrowth of graphene grain are affected by the arrangement of Cu atoms and grains because graphene growth involves the assembly of the dehydrogenated carbon radicals in energetically-favorable sites on top of the Cu lattice [37]. For example, Murdock et al. demonstrated that at LPCVD condition, shape and orientation of graphene grains change conforming to the grain orientation of Cu [38]. Luo et al. achieved adlayer-free single-crystal graphene using Cu(111) foil [39] and concluded that the significantly lower carbon content inside the Cu(111) foil compared to the commercially available polycrystalline Cu foils is the main factor in eliminating the growth of adlayers. It is well-known that the (111) facet promotes an epitaxial-like growth of graphene [26] attributing to an extremely small mismatch in their lattice constants [24,25]. The XRD of as-received Cu foil, before graphene growth, indicated that grains were either completely (α and α_{pure}) or predominantly (σ) oriented along the (200) direction. σ Cu hosted 31 and 10% of grains oriented along the (111) and (220) direction, respectively (blue trace in Fig. 2a). The low temperature annealing, 1000 °C for 1 h, similar to the typical Cu annealing during graphene crystallization by LPCVD, does not alter the grain orientation significantly (red traces in Fig. 2). Therefore, the typical short annealing of Cu foil carried out for the conventional LPCVD synthesis of graphene at 1000 °C is not sufficient to obtain Cu(111). Since the graphene grown on the σ Cu had the highest defect density (Fig. 1c), we hypothesize that the possible cause could be a less-perfect intergrowth of the graphene grains when the underlying Cu grains have a varying orientation. In other words, a single crystallographic orientation of Cu could improve the intergrowth of graphene grains, lowering the grain-boundary defects. Upon high-temperature annealing, all Cu foils converted to (111) out-of-plane orientation irrespective of their prior orientation (orange traces in Fig. 2). The top side as well as the bottom side of the annealed Cu foil indicated (111) out-of-plane orientation (Fig. S5), indicating that the whole Cu foil was transformed by the annealing process.

During the high-temperature annealing, the Cu foil was heated to 1077 °C, near its melting point of 1083 °C, and was subsequently slowly cooled to 1000 °C to provide enough time for a uniform grain growth and reorientation to Cu(111) attributing to the fact that the (111) facet has the lowest surface energy compared to the other facets [40,41]. Confirming our prior hypothesis, the single crystallographic orientation of annealed low-purity Cu, (111) in this case, significantly reduced the defect density in graphene (Fig. 1c). We note that there are several other advantages of synthesizing graphene on the (111) facet of Cu. A lower adsorption and decomposition energy for CH_4 [42], and a higher rate of

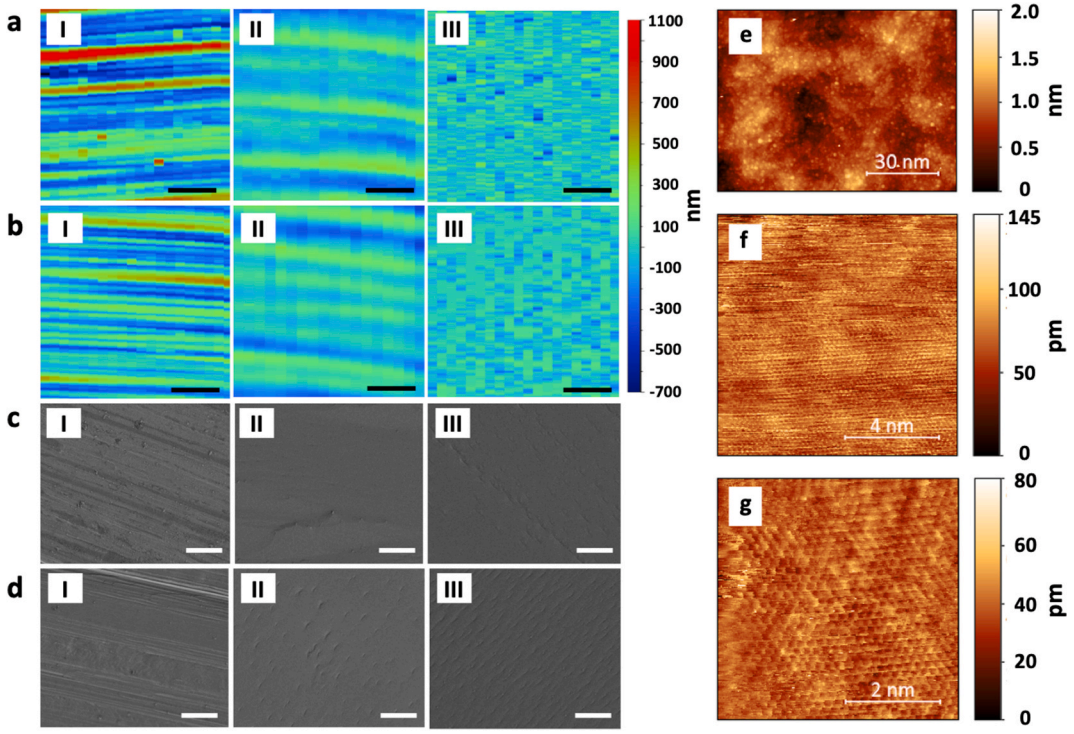

Fig. 3. Profilometer-based surface topography for σ (a) and α (b) foils. Panels I and II refer to as-received, and high-temperature annealed foils, respectively. Panel III refers to foil treated to high-temperature annealing, polishing, and high-temperature annealing in a sequential manner. The scale-bar is 50 μm. The corresponding SEM images for σ (c) and α (d) foils with a scale-bar of 3 μm. STM images of the α-A_H foil displaying the overall smoothness (e), and atomic lattice of Cu (f and g). A bias voltage of 1 V and a tunneling current of 0.2 nA was used for image in panel (e). For images in panels (f) and (g), a bias voltage of 0.1 V and a tunneling current of 0.2 nA was used.

carbon diffusion on the Cu surface [24] favors graphene growth. The thermal expansion coefficients of graphene and Cu have the lowest mismatch, and the interfacial interaction is highest when Cu possesses (111) orientation [43]. As a result, the folds and wrinkles in graphene are much reduced on Cu(111) [44]. For instance, Ogawa et al. [24] verified that the graphene grains grown on Cu(111) are mostly aligned, yet the graphene grains grown on Cu(100) possess two orientations rotated by 30°, resulting in a higher defect density. We note that the weight loss of Cu foil during the high temperature, ambient-pressure annealing was insignificant (0.21%).

3.3. Surface morphology of Cu

It is well known that decreasing the surface roughness of Cu reduces the density of graphene nucleation site, subsequently increasing the grain size of graphene [26,45]. Thereby, this can decrease the grain-boundary defects. The as-received commercial Cu foils are rough, attributed to the rolling methods involved in the production of thin foils. Usually, a short annealing of Cu foil is carried out at 1000 °C prior to the graphene growth, however, it does not lead to a significant reduction in the surface roughness. The waviness formed in Cu foil by the rolling process remains intact during the 1000 °C annealing (Fig. S6). In contrast, the high-temperature annealing process improved the surface roughness significantly (Fig. 3) with low-purity Cu foils becoming

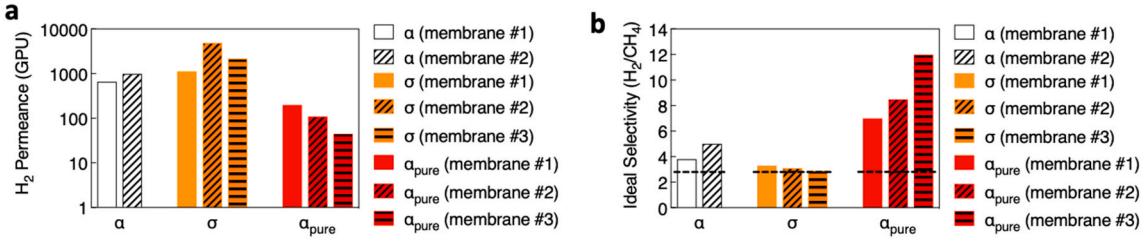

Fig. 4. H_2 permeance (a) and H_2/CH_4 ideal selectivities (b) at 25 °C from as-synthesized graphene using low-purity and high-purity Cu foils. The data on high-purity Cu, α_{pure}, is taken from literature [20].

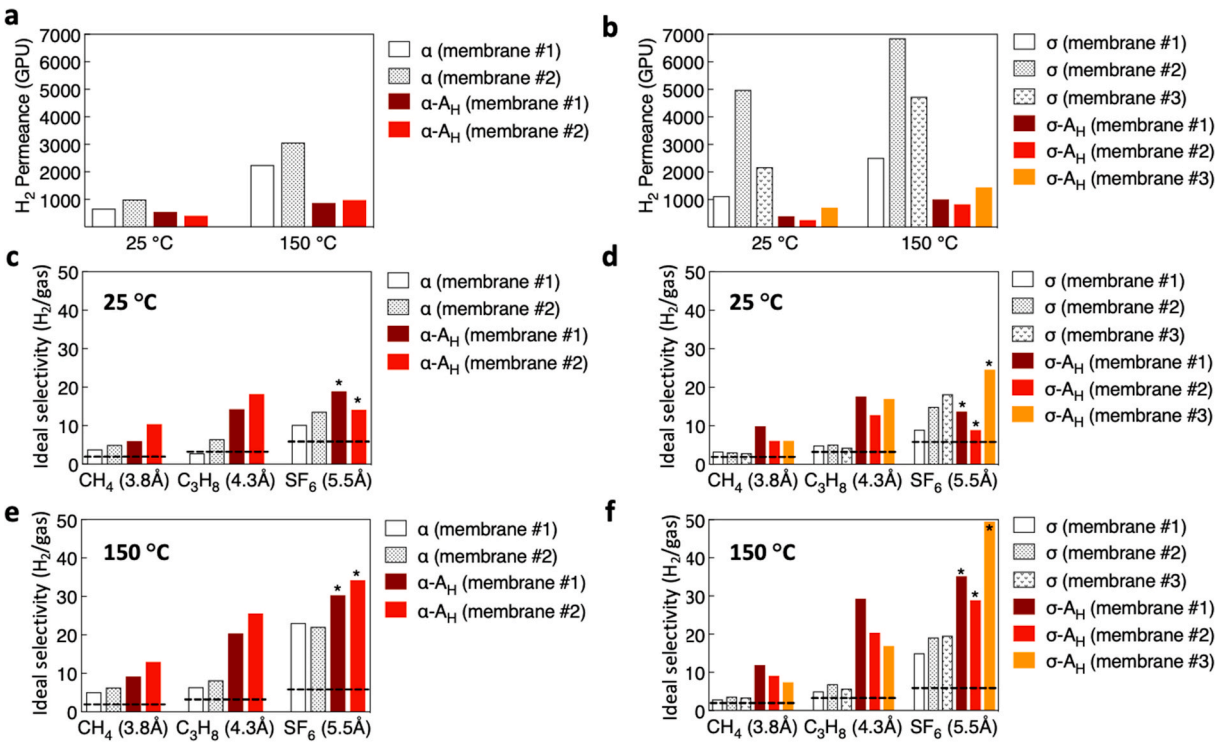

Fig. 5. H_2 permeance (a, b) and the ideal selectivities (c, d, e, f) from graphene membranes synthesized using various Cu foils. The horizontal dashed line in panels (c), (d), (e), and (f) correspond to the Knudsen selectivity for a given gas pair. The data marked with '*' indicate that the SF_6 permeance was lower than detection limit of the permeation setup, and the selectivities are calculated based on the detection limit of mass spectrometer.

visibly shiny after this step. For example, the surface roughness of the as-received α and σ foils were 206 and 320 nm, respectively (panel I in Fig. 3a–d, Table S1). After a single high-temperature annealing step, the corresponding roughness reduced to 99 and 130 nm, respectively (panel II in Fig. 3a–d, Table S1). Interestingly, the surface roughness in a single Cu step, decreased considerably, to 0.23 nm, and atomic resolution STM images could be obtained (Fig. 3c–f). The measured lattice constant, 0.22 nm, agrees well with that from the (111) orientation [46].

The Cu surface could be further smoothened by mechanical polishing. The treatment was repeated in the following sequence: high-temperature annealing, polishing and finally high-temperature annealing. This led to the complete eradication of the Cu waviness, and the surface roughness of α and σ foils reduced to 68 and 79 nm, respectively (Table S1). The size of the Cu grains increased significantly after this treatment, increasing from ca. 100 μm to ca. 340 μm (Fig. S7). Bigger Cu grains are desired because grain boundaries can obstruct the epitaxial interaction between graphene and Cu(111) [43]. However, we observed residues on Cu foil from the polishing step (Fig. S8). It was not possible to completely remove these residues by washing or sonicating the polished Cu. These residues are detrimental for the application of graphene in membranes especially when the graphene membranes are prepared by reinforcement with the fragile carbon film [20] because the carbon film tends to crack when deposited on top of the residues. We envision that with further development in the residue-free polishing step, the lower surface roughness in the α-A_H-P-A_H or σ-A_H-P-A_H foils will be advantageous for the synthesis of graphene membranes. A potential residue-free polishing step is chemical polishing or electropolishing [30]. Here, Cu atoms from the surface are dissolved reducing the surface roughness. However, electropolishing tends to reduce the graphene nucleation density to as low as 1 nuclei/mm^2. For a short crystallization time, a low nucleation density can lead to imperfect intergrowth of graphene grains, pinholes, etc. On the other hand, for a long crystallization time of graphene, multilayer graphene coverage can increase substantially.

3.4. Gas separation performance from intrinsic vacancy-defects in graphene

We recently demonstrated that the intrinsic defects in LPCVD-derived single-layer graphene are composed of subnanometer-sized carbon vacancies or nanopores and can be applied to differentiate gas molecules based on their size [20]. However, the expensive high-purity Cu foil, α_{pure}, is generally needed to achieve the needed pore-size-distribution to differentiate molecules based on their size, and the use of other low-purity foils does not result in a good selectivity (Fig. 4). Here, ideal selectivity between a gas pair is defined as the ratio of gas permeance from the single-component permeance test. Given the reorientation of Cu grains to Cu(111) (Fig. 2) accompanying a significant improvement in the surface roughness by a single high-temperature annealing step (Fig. 3), we studied the gas separation performance of graphene derived from all commercial low-purity foils. For this, 2–3 graphene membranes were fabricated from every type of commercial low-purity Cu foil.

Overall, the high-temperature annealing of the Cu foil led to graphene membranes with lower H_2 permeance (Fig. 5a and b) and increased selectivities of H_2 with respect to CH_4 and C_3H_8 (Fig. 5c–f), indicating that there were fewer nonselective vacancy-defects in graphene synthesized on the annealed foil. For example, the ideal selectivities obtained from the membrane synthesized on as-received Cu were close to those expected by the Knudsen diffusion mechanism (2.8, 4.7, and 8.0 for H_2/CH_4, H_2/C_3H_8, and H_2/SF_6, respectively, Fig. 5b, c, e, and f). Knudsen transport is typically observed when a number of nanopores are larger than the size of gas molecules [47]. In turn, larger nanopores have origin in poorly stitched grains of graphene attributing to the non-uniform crystallographic orientation of the Cu grains (Fig. 2) and the surface roughness of the foil (Fig. 3). Moreover, the as-received α-Cu membranes display lower permeance and higher selectivity, and thus higher graphene quality, than that of made by as-received σ-Cu due to a) lower surface roughness of α Cu foil, and b) single crystallographic

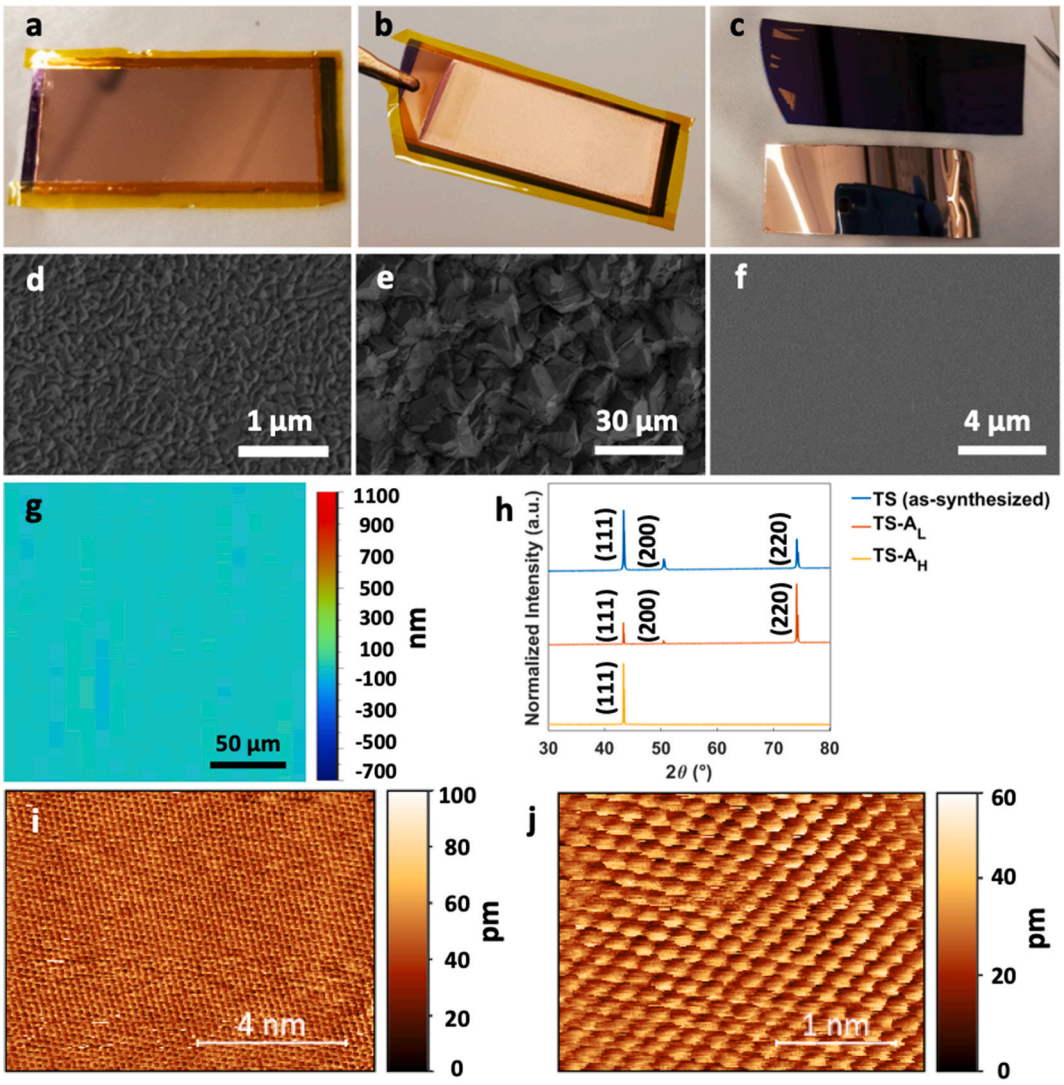

Fig. 6. Optical and SEM images of the thermally deposited (TD) Cu film on SiO_2/Si wafer (a and d), electrodeposited (ED) Cu film on TD Cu film (b and e), and peeled-off TD-ED Cu facing the SiO_2/Si wafer (c and f). g) Surface roughness measurement of the peeled-off TD-ED Cu film. h) XRD patterns of as-synthesized, annealed at 1000 °C, and exposed to high-temperature annealing template-stripping (TS) Cu foil. i, j) Atomic resolution STM images (bias voltage of 0.1V and tunneling current of 0.2 nA) of the ultra-flat TS exposed to high-temperature annealing.

orientation (200) of as-received α-Cu compared to mixed orientation in as-received σ-Cu.

The high-temperature annealing of Cu foil allowed us to realize an attractive combination of H_2 permeance and ideal selectivities from graphene synthesized on low-cost low-purity Cu foils. For example, H_2 permeance above 1000 GPU (1 GPU = 3.35×10^{-10} mol m^{-2} s^{-1} Pa^{-1}) in combination with H_2/CH_4 and H_2/C_3H_8 selectivities of 12 and 29, respectively, was realized at the permeation temperature of 150 °C for σ-A_H foil (Table S2). We did not detect the transport of SF_6 (kinetic diameter 5.5 Å) from these membranes.

We note that the ideal selectivity observed here comes from molecular-sized vacancy defects in graphene and not from the NPC film which hosts 20–30 nm sized pores [20]. The observed selectivity does not arise from graphene/NPC interface, otherwise, the selectivity and gas permeance would not be the function of porosity and pore-size-distribution in graphene [10]. To prove this further, we made two membranes utilizing PTMSP-assisted method from graphene. Permeance and selectivities of these membranes are similar to those made from utilizing the NPC-assisted method (Fig. S9).

We also note that the graphene defects studied here do not have origin in the pyrolysis to form NPC film (500 °C in the H_2/Ar atmosphere). Rather, these are intrinsic defects incorporated in the lattice during crystallization at 1000 °C. To prove this, we compared Raman mapping data from as-synthesized graphene to that from graphene placed in the pyrolysis condition for 1 h (Fig. S10). We did not find any significant change in defect density. The Raman mapping measurements were done on the same area of the sample for all three measurements.

The separation of H_2 from hydrocarbons makes these membranes attractive for application in off-gas recovery in the petrochemical industry. The gas transport results are in good agreement with the Raman spectroscopy measurements demonstrating a significant improvement in graphene quality on par with the previously reported graphene membranes synthesized on expensive high-purity Cu foils [20].

The synthesis of high-quality graphene with control over pore-size-distribution of the intrinsic vacancy defects has a paramount importance to the ongoing efforts on the incorporation of high-density of nanopores in graphene by the postsynthetic etching of graphene lattice to obtain large yet selective gas permeance. Generally, the intrinsic vacancy-defects are expected to expand into large nonselective nanopores during the postsynthetic etching of graphene lattice. However, high selectivity can be obtained by postsynthetic etching if the density of

Table 1
Comparisons of the Cu foil and resulting graphene membranes after the annealing step.

Sample	Treatment	Cu crystallographic orientation	Overall RMS (nm)	I_D/I_G (graphene)	H_2 permeance (GPU)	H_2/CH_4 ideal selectivity
α purity = 99.8%	As-received	(200)	206	0.07 ± 0.02	2655	5.7
	Annealed	(111)	99	0.06 ± 0.01	925	11.1
σ purity = 99.98%	As-received	mixed	252	0.18 ± 0.02	4700	3.3
	Annealed	(111)	105	0.10 ± 0.01	1090	9.5
TS	As-made	mixed	<15	0.04 ± 0.01	–	–
	Annealed	(111)	85	0.04 ± 0.01	–	–
α_{pure} purity 99.999%	As-received	(200)	124	0.04 ± 0.01	600	11.3

freshly etched nanopores are significantly higher than that of intrinsic vacancy defects [10,48,49]. This study on crystallographic and morphological optimization of Cu foil contributes to this cause by i) reducing the density of the intrinsic vacancy defects (Fig. 1c; Fig. 5a and b), and ii) reducing the average size of the intrinsic vacancy defects (Fig. 5c–f).

3.5. In-house synthesis of smooth high-purity Cu(111) foils

The above results reveal that smoothened Cu(111) substrates significantly improve the quality of the graphene membranes. To further improve the smoothness of the foil, we prepared Cu foil by the template-stripping (TS) process [27]. For this, ca. 1-μm-thick Cu film was deposited on a Si/SiO_2 wafer by a thermal evaporator (Fig. 6a, d). Next, a 25-μm-thick Cu film was electrodeposited (ED) on top of the thermally-deposited (TD) Cu film to improve the mechanical robustness of the film for the subsequent graphene synthesis step (Fig. 6b, e). An extremely smooth and shiny surface, with a local surface roughness of 0.19 Å, on a single Cu step measured by STM, was obtained by peeling off the Cu foil (Fig. 6c, f, and g). The grains in the as-synthesized foils were not uniformly oriented, however, they had a preference towards the (111) facet, in agreement with the literature (Fig. 6h). The grain orientation was more or less maintained during the graphene synthesis where the foil was annealed at 1000 °C. However, similar to the observation with the commercial foils, the grain orientation converted entirely to (111) after the high-temperature annealing. Even after annealing, the foil retained its local smoothness, and atomic-resolution images could be obtained (Fig. 6i and j). Consistent with the prior observations, the combination of (111) grain orientation and extremely smooth surface led to the lowest defect-density in graphene (I_D/I_G = 0.04 ± 0.01) among all the samples in this study. These homemade foils will be highly attractive for the synthesis of graphene membranes. We observed that the presence of unavoidable dust particles on the Si wafer in the normal laboratory conditions led to the generation of micron-sized pinholes on the Cu surface with a population of 1–2 pinhole/mm^2 (Fig. S11). Performing the synthesis in a dust-free environment should eliminate the problem.

To understand the overall effect of high-temperature annealing step which improves the RMS roughness, and orients the Cu foil to (111), leading to improvement in H_2/CH_4 selectivity, the corresponding data is summarized in Table 1. There is a clear correlation of high-temperature annealing with the lowering of defect density (I_D/I_G), orientation change of Cu foils to (111), reduction of RMS, reduction of hydrogen permeance, and the increase in H_2/CH_4 selectivity. The reduction of RMS roughness always lowered down the defect density and improved the membrane performance. However, there is a weak or no correlation of defects and membrane performance with the Cu purity. This could be attributed to the fact that the typical impurities in Cu consist of other metals. During the high-temperature annealing near the melting point of Cu, a liquid Cu layer is present on the surface of the foil which may form a high-purity Cu top-layer. This hypothesis will be confirmed by systematic experiments in future studies. Overall, the most important parameter for the improvement of the graphene membrane on low-cost Cu foil was the improvement of RMS roughness by high-temperature annealing.

4. Conclusions

In conclusion, a facile crystallographic and morphological optimization protocol for commercial low-cost Cu foil is demonstrated which led to the CVD of single-layer graphene hosting hydrogen-sieving intrinsic defects. The slow annealing reported in this study proved much more effective than the usual annealing of Cu foil that invariably takes place during the graphene synthesis. This was evident in the crystallographic changes where the Cu foil orientation changes to (111) only upon the slow-annealing method. The RMS roughness of the high-temperature-annealed Cu foil reduced significantly to ca. 100 nm. The improved smoothness of the Cu foil was the most important factor in achieving better H_2/CH_4 and H_2/SF_6 selectivities. Interestingly, no particular trend was observed with respect to the purity of the Cu foil, which could help to extend the current method to other low-purity foils. We speculate that this could be because of the formation of a high-purity Cu top layer after the high-temperature annealing step. Finally, the ability of carry out atomic-resolution STM imaging on smoothened Cu foils will help future STM studies on understanding the structure of vacancy-defects in graphene.

Author contributions

K·V.A. and M.R. conceived the project and wrote the paper. M.R. built the CVD setup and performed the experiments. M. R. and S. L. did the STM studies. S.H. assisted with the NPC-based graphene transfer and developing the annealing method. All authors revised the paper.

Declaration of competing interest

The authors declare that they have no known competing financial interests or personal relationships that could have appeared to influence the work reported in this paper.

CRediT authorship contribution statement

Mojtaba Rezaei: Conceptualization, Formal analysis, Writing - review & editing. **Shaoxian Li:** Investigation, Formal analysis. **Shiqi Huang:** Conceptualization, Investigation, Formal analysis. **Kumar Varoon Agrawal:** Conceptualization, Writing - review & editing.

Acknowledgments

The authors acknowledge the host institution, EPFL, for the generous support. This project was funded by the Swiss National Science Foundation under the Assistance Professor Energy Grant (grant number PYAPP2_173645). A part of this work was funded by European Research Council Starting Grant (grant number 804537). SH and SL thank GAZNAT for funding a part of the project.

Appendix A. Supplementary data

Supplementary data to this article can be found online at https://doi.org/10.1016/j.memsci.2020.118406.

References

[1] L. Wang, L.W. Drahushuk, L. Cantley, S.P. Koenig, X. Liu, J. Pellegrino, M.S. Strano, J. Scott Bunch, Molecular valves for controlling gas phase transport made from discrete ångström-sized pores in graphene, Nat. Nanotechnol. 10 (2015) 785–790, https://doi.org/10.1038/nnano.2015.158.

[2] S.P. Koenig, L. Wang, J. Pellegrino, J.S. Bunch, Selective molecular sieving through porous graphene, Nat. Nanotechnol. 7 (2012) 728–732, https://doi.org/10.1038/nnano.2012.162.

[3] L. Wang, M.S.H. Boutilier, P.R. Kidambi, D. Jang, N.G. Hadjiconstantinou, R. Karnik, Fundamental transport mechanisms, fabrication and potential applications of nanoporous atomically thin membranes, Nat. Nanotechnol. 12 (2017) 509–522, https://doi.org/10.1038/nnano.2017.72.

[4] A. Kaplan, Z. Yuan, J.D. Benck, A. Govind Rajan, X.S. Chu, Q.H. Wang, M.S. Strano, Current and future directions in electron transfer chemistry of graphene, Chem. Soc. Rev. (2017), https://doi.org/10.1039/C7CS00181A.

[5] K.V. Agrawal, L.W. Drahushuk, M.S. Strano, Observation and analysis of the Coulter effect through carbon nanotube and graphene nanopores, Philos. Trans. R. Soc. A Math. Phys. Eng. Sci. 374 (2016) 20150357, https://doi.org/10.1098/rsta.2015.0357.

[6] Z. Yuan, A. Govind Rajan, R.P. Misra, L.W. Drahushuk, K.V. Agrawal, M.S. Strano, D. Blankschtein, Mechanism and prediction of gas permeation through sub-nanometer graphene pores: comparison of theory and simulation, ACS Nano 11 (2017) 7974–7987, https://doi.org/10.1021/acsnano.7b02523.

[7] D.E. Jiang, V.R. Cooper, S. Dai, Porous graphene as the ultimate membrane for gas separation, Nano Lett. 9 (2009) 4019–4024, https://doi.org/10.1021/Nl9021946.

[8] Z. Yuan, R.P. Misra, A.G. Rajan, M.S. Strano, D. Blankschtein, Analytical prediction of gas permeation through graphene nanopores of varying sizes: understanding transitions across multiple transport regimes, ACS Nano 13 (2019) 11809–11824, https://doi.org/10.1021/acsnano.9b05779.

[9] S.C. O'Hern, M.S.H. Boutilier, J.C. Idrobo, Y. Song, J. Kong, T. Laoui, M. Atieh, R. Karnik, Selective ionic transport through tunable subnanometer pores in single-layer graphene membranes, Nano Lett. 14 (2014) 1234–1241, https://doi.org/10.1021/nl404118f.

[10] J. Zhao, G. He, S. Huang, L.F. Villalobos, M. Dakhchoune, H. Bassas, K.V. Agrawal, Etching gas-sieving nanopores in single-layer graphene with an angstrom precision for high-performance gas mixture separation, Sci. Adv. 5 (2019) eaav1851, https://doi.org/10.1126/sciadv.aav1851.

[11] X. Li, W. Cai, J. An, S. Kim, J. Nah, D. Yang, R. Piner, A. Velamakanni, I. Jung, E. Tutuc, S.K. Banerjee, L. Colombo, R.S. Ruoff, Large-area synthesis of high-quality and uniform graphene films on copper foils, Science 324 (2009) 1312–1314, https://doi.org/10.1126/science.1171245.

[12] X. Li, W. Cai, L. Colombo, R. Ruoff, Evolution of graphene growth on Ni and Cu by carbon isotope labeling, Nano Lett. 12 (2009) 1–15. http://pubs.acs.org/doi/abs/10.1021/nl902515k.

[13] S. Bae, H. Kim, Y. Lee, X. Xu, J.-S. Park, Y. Zheng, J. Balakrishnan, T. Lei, H. Ri Kim, Y. Il Song, Y.-J. Kim, K.S. Kim, B. Özyilmaz, J.-H. Ahn, B.H. Hong, S. Iijima, Roll-to-roll production of 30-inch graphene films for transparent electrodes, Nat. Nanotechnol. 5 (2010) 574–578, https://doi.org/10.1038/nnano.2010.132.

[14] P.R. Kidambi, D.D. Mariappan, N.T. Dee, A. Vyatskikh, S. Zhang, R. Karnik, A. J. Hart, A scalable route to nanoporous large-area atomically thin graphene membranes by roll-to-roll chemical vapor deposition and polymer support casting, ACS Appl. Mater. Interfaces 10 (2018) 10369–10378, https://doi.org/10.1021/acsami.8b00846.

[15] X. Li, C.W. Magnuson, A. Venugopal, R.M. Tromp, J.B. Hannon, E.M. Vogel, L. Colombo, R.S. Ruoff, Large-area graphene single crystals grown by low-pressure chemical vapor deposition of methane on copper, J. Am. Chem. Soc. 133 (2011) 2816–2819, https://doi.org/10.1021/ja109793s.

[16] X. Xu, Z. Zhang, L. Qiu, J. Zhuang, L. Zhang, H. Wang, C. Liao, H. Song, R. Qiao, P. Gao, Z. Hu, L. Liao, Z. Liao, D. Yu, E. Wang, F. Ding, H. Peng, K. Liu, Ultrafast growth of single-crystal graphene assisted by a continuous oxygen supply, Nat. Nanotechnol. 11 (2016) 1–13, https://doi.org/10.1038/nnano.2016.132.

[17] J. Červenka, C.F.J. Flipse, Structural and electronic properties of grain boundaries in graphite: planes of periodically distributed point defects, Phys. Rev. B Condens. Matter 79 (2009) 1–5, https://doi.org/10.1103/PhysRevB.79.195429.

[18] J. Coraux, A.T. N'Diaye, M. Engler, C. Busse, D. Wall, N. Buckanie, F.J. Meyer Zu Heringdorf, R. Van Gastel, B. Poelsema, T. Michely, Growth of graphene on Ir (111), New J. Phys. 11 (2009), https://doi.org/10.1088/1367-2630/11/2/023006.

[19] K.V. Agrawal, J.D. Benck, Z. Yuan, R.P. Misra, A. Govind Rajan, Y. Eatmon, S. Kale, X.S. Chu, D.O. Li, C. Gong, J. Warner, Q.H. Wang, D. Blankschtein, M.S. Strano, Fabrication, pressure testing, and nanopore formation of single-layer graphene membranes, J. Phys. Chem. C 121 (2017) 14312–14321, https://doi.org/10.1021/acs.jpcc.7b01796.

[20] S. Huang, M. Dakhchoune, W. Luo, E. Oveisi, G. He, M. Rezaei, J. Zhao, D.T. L. Alexander, A. Züttel, M.S. Strano, K.V. Agrawal, Single-layer graphene membranes by crack-free transfer for gas mixture separation, Nat. Commun. 9 (2018) 1–11, https://doi.org/10.1038/s41467-018-04904-3.

[21] P.R. Kidambi, G.D. Nguyen, S. Zhang, Q. Chen, J. Kong, J. Warner, A.P. Li, R. Karnik, Facile fabrication of large-area atomically thin membranes by direct synthesis of graphene with nanoscale porosity, Adv. Mater. (2018) 1804977, https://doi.org/10.1002/adma.201804977, 1–10.

[22] Z. Yuan, J.D. Benck, Y. Eatmon, D. Blankschtein, M.S. Strano, Stable, temperature-dependent gas mixture permeation and separation through suspended nanoporous single-layer graphene membranes, Nano Lett. 18 (2018) 5057–5069, https://doi.org/10.1021/acs.nanolett.8b01866.

[23] M.H. Khan, M. Moradi, M. Dakhchoune, M. Rezaei, S. Huang, J. Zhao, K. V. Agrawal, Hydrogen sieving from intrinsic defects of benzene-derived single-layer graphene, Carbon N. Y. 153 (2019) 458–466, https://doi.org/10.1016/j.carbon.2019.07.045.

[24] Y. Ogawa, B. Hu, C.M. Orofeo, M. Tsuji, K. Ikeda, S. Mizuno, H. Hibino, H. Ago, Domain structure and boundary in single-layer graphene grown on Cu(111) and Cu (100) films, J. Phys. Chem. Lett. 3 (2012) 219–226, https://doi.org/10.1021/jz2015555.

[25] H. Ago, Y. Ogawa, M. Tsuji, S. Mizuno, H. Hibino, Catalytic growth of graphene: toward large-area single-crystalline graphene, J. Phys. Chem. Lett. 3 (2012) 2228–2236, https://doi.org/10.1021/jz3007029.

[26] H.K. Yu, K. Balasubramanian, K. Kim, J.-L. Lee, M. Maiti, C. Ropers, J. Krieg, K. Kern, A.M. Wodtke, Chemical vapor deposition of graphene on a "peeled-off" epitaxial Cu(111) foil: a simple approach to improved properties, ACS Nano 8 (2014) 8636–8643, https://doi.org/10.1021/nn503476j.

[27] P. Procházka, J. Mach, D. Bischoff, Z. Lišková, P. Dvořák, M. Vaňatka, P. Simonet, A. Varlet, D. Hemzal, M. Petrenec, L. Kalina, M. Bartošík, K. Ensslin, P. Varga, J. Čechal, T. Šikola, Ultrasmooth metallic foils for growth of high quality graphene by chemical vapor deposition, Nanotechnology 25 (2014), https://doi.org/10.1088/0957-4484/25/18/185601.

[28] G. He, S. Huang, L.F. Villalobos, J. Zhao, M. Mensi, E. Oveisi, M. Rezaei, K. V. Agrawal, High-permeance polymer-functionalized single-layer graphene membranes that surpass the postcombustion carbon capture target, Energy Environ. Sci. (2019) 12–16, https://doi.org/10.1039/c9ee01238a.

[29] Y. Hao, M.S. Bharathi, L. Wang, Y. Liu, H. Chen, S. Nie, X. Wang, H. Chou, C. Tan, B. Fallahazad, H. Ramanarayan, C.W. Magnuson, E. Tutuc, B.I. Yakobson, K. F. McCarty, Y.-W. Zhang, P. Kim, J. Hone, L. Colombo, R.S. Ruoff, The role of surface oxygen in the growth of large single-crystal graphene on copper, Science 342 (2013) 720–723, https://doi.org/10.1126/science.1243879.

[30] Z. Yan, J. Lin, Z. Peng, Z. Sun, Y. Zhu, L. Li, C. Xiang, E.L. Samuel, C. Kittrell, J. M. Tour, Toward the synthesis of wafer-scale single-crystal graphene on copper foils, ACS Nano 6 (2012) 9110–9117, https://doi.org/10.1021/nn303352k.

[31] V.L. Nguyen, B.G. Shin, D.L. Duong, S.T. Kim, D. Perello, Y.J. Lim, Q.H. Yuan, F. Ding, H.Y. Jeong, H.S. Shin, S.M. Lee, S.H. Chae, Q.A. Vu, S.H. Lee, Y.H. Lee, Seamless stitching of graphene domains on polished copper (111) foil, Adv. Mater. 27 (2015) 1376–1382, https://doi.org/10.1002/adma.201404541.

[32] L. Brown, E.B. Lochocki, J. Avila, C.J. Kim, Y. Ogawa, R.W. Havener, D.K. Kim, E. J. Monkman, D.E. Shai, H.I. Wei, M.P. Levendorf, M. Asensio, K.M. Shen, J. Park, Polycrystalline graphene with single crystalline electronic structure, Nano Lett. 14 (2014) 5706–5711, https://doi.org/10.1021/nl502445j.

[33] L.G. Cançado, A. Jorio, E.H.M. Ferreira, F. Stavale, C.A. Achete, R.B. Capaz, M.V. O. Moutinho, A. Lombardo, T.S. Kulmala, A.C. Ferrari, Quantifying defects in graphene via Raman spectroscopy at different excitation energies, Nano Lett. 11 (2011) 3190–3196, https://doi.org/10.1021/nl201432g.

[34] A.C. Ferrari, D.M. Basko, Raman spectroscopy as a versatile tool for studying the properties of graphene, Nat. Nanotechnol. 8 (2013) 235–246, https://doi.org/10.1038/nnano.2013.46.

[35] I. Ruiz, W. Wang, A. George, C.S. Ozkan, M. Ozkan, Silicon oxide contamination of graphene sheets synthesized on copper substrates via chemical vapor deposition, Adv. Sci. Eng. Med. 6 (2014) 1070–1075, https://doi.org/10.1166/asem.2014.1615.

[36] D. Senyildiz, O.T. Ogurtani, G. Cambaz Buke, The effects of acid pretreatment and surface stresses on the evolution of impurity clusters and graphene formation on Cu foil, Appl. Surf. Sci. 425 (2017) 873–878, https://doi.org/10.1016/j.apsusc.2017.07.092.

[37] S. Dutta, M.T. Vahdat, M. Rezaei, K.V. Agrawal, Crystallization of gas-selective nanoporous graphene by competitive etching and growth: a modeling study, Sci. Rep. 9 (2019) 1–11, https://doi.org/10.1038/s41598-019-41645-9.

[38] A.T. Murdock, A. Koos, T. Ben Britton, L. Houben, T. Batten, T. Zhang, A. J. Wilkinson, R.E. Dunin-Borkowski, C.E. Lekka, N. Grobert, Controlling the orientation, edge geometry, and thickness of chemical vapor deposition graphene, ACS Nano 7 (2013) 1351–1359, https://doi.org/10.1021/nn3049297.

[39] D. Luo, M. Wang, Y. Li, C. Kim, K.M. Yu, Y. Kim, H. Han, M. Biswal, M. Huang, Y. Kwon, M. Goo, D.C. Camacho-Mojica, H. Shi, W.J. Yoo, M.S. Altman, H.J. Shin, R.S. Ruoff, Adlayer-free large-area single crystal graphene grown on a Cu(111) foil, Adv. Mater. 1903615 (2019) 1–13, https://doi.org/10.1002/adma.201903615.

[40] C.V. Thompson, Grain growth in thin films, Annu. Rev. Mater. Sci. 20 (1990) 245–268, https://doi.org/10.1146/annurev.ms.20.080190.001333.

[41] S. Jin, M. Huang, Y. Kwon, L. Zhang, B.W. Li, S. Oh, J. Dong, D. Luo, M. Biswal, B. V. Cunning, P.V. Bakharev, I. Moon, W.J. Yoo, D.C. Camacho-Mojica, Y.J. Kim, S. H. Lee, B. Wang, W.K. Seong, M. Saxena, F. Ding, H.J. Shin, R.S. Ruoff, Colossal grain growth yields single-crystal metal foils by contact-free annealing, Science 362 (2018) 1021–1025, https://doi.org/10.1126/science.aao3373.

[42] L. Tao, J. Lee, M. Holt, H. Chou, S.J. McDonnell, D.A. Ferrer, M.G. Babenco, R. M. Wallace, S.K. Banerjee, R.S. Ruoff, D. Akinwande, Uniform wafer-scale chemical vapor deposition of graphene on evaporated Cu (111) film with quality comparable to exfoliated monolayer, J. Phys. Chem. C 116 (2012) 24068–24074, https://doi.org/10.1021/jp3068848.

[43] B. Deng, Z. Pang, S. Chen, X. Li, C. Meng, J. Li, M. Liu, J. Wu, Y. Qi, W. Dang, H. Yang, Y. Zhang, J. Zhang, N. Kang, H. Xu, Q. Fu, X. Qiu, P. Gao, Y. Wei, Z. Liu, H. Peng, Wrinkle-free single-crystal graphene wafer grown on strain-engineered substrates, ACS Nano 11 (2017) 12337–12345, https://doi.org/10.1021/acsnano.7b06196.

[44] Z. Yan, Z. Peng, J.M. Tour, Chemical vapor deposition of graphene single crystals, Acc. Chem. Res. 47 (2014) 1327–1337, https://doi.org/10.1021/ar4003043.

[45] I. Vlassiouk, S. Smirnov, M. Regmi, S.P. Surwade, N. Srivastava, R. Feenstra, G. Eres, C. Parish, N. Lavrik, P. Datskos, S. Dai, P. Fulvio, Graphene nucleation density on copper: fundamental role of background pressure, J. Phys. Chem. C 117 (2013) 18919–18926, https://doi.org/10.1021/jp4047648.

[46] H. Walen, D.J. Liu, J. Oh, H. Lim, J.W. Evans, C.M. Aikens, Y. Kim, P.A. Thiel, Cu2S3 complex on Cu(111) as a candidate for mass transport enhancement, Phys. Rev. B Condens. Matter 91 (2015) 1–7, https://doi.org/10.1103/PhysRevB.91.045426.

[47] K. Celebi, J. Buchheim, R.M. Wyss, A. Droudian, P. Gasser, I. Shorubalko, J.-I. Kye, C. Lee, H.G. Park, Ultimate permeation across atomically thin porous graphene, Science 344 (2014) 289–292, https://doi.org/10.1126/science.1249097.

[48] M.S.H. Boutilier, D. Jang, J.C. Idrobo, P.R. Kidambi, N.G. Hadjiconstantinou, R. Karnik, Molecular sieving across centimeter-scale single-layer nanoporous graphene membranes, ACS Nano 11 (2017) 5726–5736, https://doi.org/10.1021/acsnano.7b01231.

[49] M.S.H. Boutilier, C. Sun, S.C. O'Hern, H. Au, N.G. Hadjiconstantinou, R. Karnik, Implications of permeation through intrinsic defects in graphene on the design of defect-tolerant membranes for gas separation, ACS Nano 8 (2014) 841–849, https://doi.org/10.1021/nn405537u.